Impact of synthesis conditions in Na-rich Prussian Blue Analogs

Paula Sanz Camacho, Romain Wernert, Mathieu Duttine, Alain Wattiaux, Ashish Rudola, Palani Balaya, François Fauth, Romain Berthelot, L. Monconduit, Dany Carlier, et al.

Impact of synthesis conditions in Na-rich Prussian Blue Analogs

Paula Sanz Camacho [a,b,d], Romain Wernert [a,b,d], Mathieu Duttine [a], Alain Wattiaux [a], Ashish Rudola [f,g], Palani Balaya [f], François Fauth [c], Romain Berthelot [b,d], Laure Monconduit [b,d,e], Dany Carlier [a,d,e *] and Laurence Croguennec [a,d,e *]

[a] CNRS, Univ. Bordeaux, Bordeaux INP, ICMCB UMR 5026, F-33600, Pessac, France.

[b] ICGM, Univ. Montpellier, CNRS, ENSCM, F-34095 Montpellier, France

[c] CELLS-ALBA synchrotron, E-08290 Cerdanyola del Vallès, Barcelona, Spain.

[d] RS2E, Réseau Français sur le Stockage Electrochimique de l'Energie, FR CNRS 3459, F-80039 Amiens Cedex 1, France.

[e] ALISTORE-ERI European Research Institute, FR CNRS 3104, Amiens, F-80039 Cedex 1, France.

[f] Department of Mechanical Engineering, National University of Singapore, 117576, Singapore.

[g] Department of Material Science and Engineering, National University of Singapore, Singapore 117575, Singapore

* Corresponding author: D. Carlier (Dany.Carlier@icmcb.cnrs.fr)

* Corresponding author: L. Croguennec (Laurence.Croguennec@icmcb.cnrs.fr)

Abstract

Sodium rich iron hexacyanoferrates were prepared by coprecipitation, hydrothermal route, and under reflux, with or without dehydration. They were obtained with different structures described in cubic, orthorhombic or rhombohedral symmetry, with variable compositions in sodium, water and cationic vacancies, and with a variety of morphologies. This series of sodium rich Prussian Blue Analogs allowed to address the relationship between synthesis conditions, composition, structure, morphology and electrochemical properties in Na-ion batteries. A new orthorhombic phase with the $Na_{1.8}Fe_2(CN)_6 \cdot 0.7H_2O$ composition synthesized by an hydrothermal route at 140°C is reported for the first time, whereas a phase of $Na_2Fe_2(CN)_6 \cdot 2H_2O$ composition obtained under reflux, previously described with a monoclinic structure, shows in fact a rhombohedral structure.

Keywords: Na-ion batteries, Prussian Blue Analogs, Iron hexacyanoferrates, hydrothermal synthesis, coprecipitation synthesis

1. Introduction

Large-scale storage of renewable energies and their integration into the grid are keys towards sustainable energy.[1] In this context, rechargeable batteries based on low-cost, non-toxic and abundant resources are highly desired. Na-ion batteries have been proposed due the large abundance of sodium (*i.e.*, the 6th most abundant element in the earth crust) and due to their similarities to the Li–ion batteries that should promote fast technology readiness level improvement.[2, 3] Among the materials studied as positive electrodes for Na batteries, Prussian Blue Analogues (PBAs) have received enormous interest in the last 5 years as their open frameworks can accommodate a large panel of cations (Na^+, K^+, Ca^{2+}, Mg^{2+}, Sr^{2+}, Ba^{2+}) without structure collapse. [4, 5, 6, 7] In particular, the hexacyanoferrates (MHCFs, M = Fe, Mn) are the most interesting PBAs materials, due to their non-toxicity, low cost and attractive specific capacities (for instance 170 mAh.g^{-1} for $Na_2Fe_2(CN)_6$).[8, 9, 10]

The structure of PBAs consists, in the absence of vacancies and water molecules, of a double perovskite-analogue framework with the CN^- anions bridging high spin M_AN_6 and low spin M_BC_6 octahedra, while the alkali cations (here the Na^+ ions) are placed in the cavities as shown in **Figure 1**. However, depending on the synthesis conditions used, the presence of vacancies and crystalline water molecules can also be present in the structure leading to a $Na_xM_A[M_B(CN)_6]_{1-y}\square_y \cdot nH_2O$ chemical formula, where M_A and M_B are different transition metal ions, $\square_y$ the vacancies of $[M_B(CN)_6]$ and $n.H_2O$ the number of crystalline water molecules. PBAs typically crystallise in a face-centred cubic structure, however depending on the amount of Na^+ ions, interstitial water molecules and vacancies, lower symmetry phases such as monoclinic or rhombohedral have been observed. This presence of crystalline water molecules and vacancies apart of having an influence on the crystal structure, does impact also their electrochemical performance. It is therefore crucial to monitor the synthesis

conditions in order to control their composition and structure along with particles size. [9, 11, 12] In order to achieve high theoretical capacities, a great effort has been done to synthesize these materials as sodium rich phases, with small content of water molecules and vacancies.[13, 14, 15]

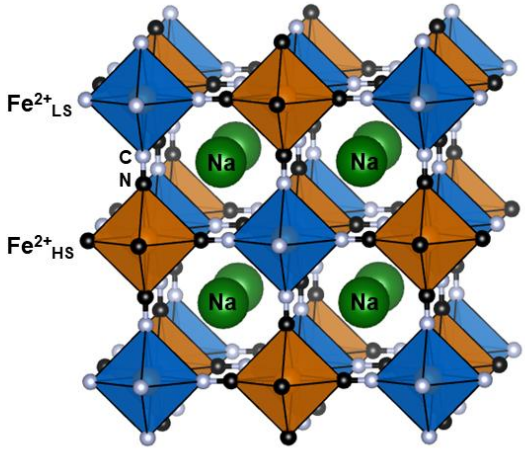

Figure 1 : Schematic illustration of the ideal structure of PBA, here $Na_2Fe_2(CN)_6$. The $Fe^{2+}_{LS}C_6$ and $Fe^{2+}_{HS}N_6$ octahedra are given as blue and orange polyhedra, respectively. The Na^+ ions, represented by green spheres, occupy the cavities of the structure.

In literature, materials prepared with the $Na_2Fe_2(CN)_6$ target composition are reported to crystallize in three different polymorphs, with rhombohedral, cubic or monoclinic unit cell symmetry (for $Na_xFe_2(CN)_6$ final composition with $x \geq 1.70$). Specific capacities up to 140 mAh/g have been reported for Na_xFeHCF ($x \geq 1.70$). [16-18]

In this work, we chose to investigate these three $Na_xFe_2(CN)_6$, where x~2 [16-18] polymorphs in order to better understand the relationship between synthesis conditions, composition, structure and electrochemical properties. In addition to X-ray powder diffraction (XRPD) characterization technique that provides information on the long range average structure, we also analysed the local structure of the materials by ^{57}Fe Mössbauer spectroscopy. It is worth mentioning that for the ideal $Na_2Fe_2(CN)_6$ compound, only two different Fe environments are

expected: $Fe^{2+}_{LS}C_6$ and $Fe^{2+}_{HS}N_6$ octahedra as shown in **Figure 1** (LS and HS for low spin and high spin respectively). In Na deficient compounds (Na/Fe ratio < 1), additional Fe environments are expected since Fe^{3+} ions are formed due to charge compensation. This technique hence gives information on the local environments of Fe (number of sites, distortion, disorder, oxidation states), but is also very informative to establish the Na composition of the materials.

In our study, we selected two synthesis routes: the precipitation and hydrothermal routes with different temperature conditions. The variation of the reaction temperature has been shown to have an impact on the composition, structure and electrochemical performances of the materials. Moreover, we succeed to prepare a new Na rich $Na_xFe_2(CN)_6$ polymorph with an orthorhombic cell, that was not yet reported in literature to the best of our knowledge. The structure and electrochemical properties of this phase will be discussed in comparison with the three other polymorphs.

2. Experimental method

Synthesis. A series of Prussian Blue Analogs $Na_xM_A[M_B(CN)_6]_{1-y}\square_y \cdot nH_2O$ (M_A = M_B = Fe) has been prepared using different synthesis routes (coprecipitation or hydrothermal) and at different temperatures. In the following, the materials will be named accordingly, such as for instance Na-FeHCF-Cop-60°C which is obtained by a coprecipitation route at 60°C.

The synthesis of Na-FeHCF-Cop-60°C material has been inspired by the work of Piernas-Munoz *et al.*[17] The initial aqueous solution, solution A, containing a mixture of $Na_4Fe(II)(CN)_6.10H_2O$ (Sigma-Aldrich; ≥ 99%) (40 mM, 100 mL), an excess of NaCl (Sigma-Aldrich; ≥ 99%) (18.9 g) and 5 mL of a solution of ascorbic acid (VWR; 100%) (45 mM, 10 mL) was heated at 60 ºC for complete dissolution. Solution A was added dropwise

using a programmable syringe pump into solution B, a pale yellow-greenish solution of $FeCl_2$ (Sigma-Aldrich; ≥ 98%) (40 mM, 100 mL) with 5 mL of the ascorbic acid solution (45 mM, 10 mL), previously heated at 60 ºC, while stirring in Ar atmosphere. After 4h stirring and heating at 60°C in Ar flow, the mixture was aged for 2 hours (just enough time to be cooled down) before being centrifuged and filtered. The product was washed with water, then with acetone and dried at 65°C. A blue dark powder was obtained. On the contrary, to the protocol described in reference 17, ascorbic acid (1.125 equivalents) was added to both solutions to slow down the nucleation as it has been recently reported by Wang *et al.*[19] Please note that the effect of ascorbic acid on the compound obtained was not explored here, as the purpose was to synthesize the cubic phase described by Piernas-Munoz *et al.*[17] as a reference, to be compared with the other phases prepared in this work.

The material Na-FeHCF-reflux-107°C was obtained from the mixture of $Na_4Fe(CN)_6$ with an excess of ascorbic acid (4.5 equivalents) heated under reflux at 107°C using an oil bath, as described in reference [18]. The material Na-FeHCF-Vac-220°C was obtained by dehydration, heating the previous material 2h at 220°C in vacuum ($2 \cdot 10^{-2}$ hPa).[18]

The Na-FeHCF-hyd-60°C, Na-FeHCF-hyd-107°C and Na-FeHCF-hyd-140°C materials were obtained through an hydrothermal route inspired by the work of Wang *et al.*[16] However, in contrast to their results which report a pH of 6.5, in our case a pH value of 3 was required to perform the reaction with success, therefore with an excess of ascorbic acid (4.5 equivalents). It is worth mentioning that using a pH of 6.5, we obtained only Fe_2O_3. Ascorbic acid (225 mM) was rapidly added to an aqueous solution of $Na_4Fe(II)(CN)_6$ $10H_2O$ (Sigma-Aldrich; ≥ 99%) (50 mM, 100 mL), and the mixture was left stirring until complete dissolution. The mixture was then transferred into an autoclave and heated in different conditions: 60, 107 or 140°C overnight. In each case, the resulting suspension was then washed with water and acetone and dried at 80°C in an oven. Blue-intense powders were obtained for Na-FeHCF-

hyd-60°C and Na-FeHCF-hyd-107°C, while a pale-green powder was obtained for Na-FeHCF-hyd-140°C.

Structural characterization. Laboratory powder X-ray diffraction (XRD) patterns were either collected on a PANAlytical X'pert PRO MPD diffractometer in Bragg-Brentano θ-θ geometry equipped with a secondary monochromator and X'Celerator multi-strip detector, or using a PANalytical XPert 3 diffractometer in Debye-Scherrer θ-θ configuration, and both equipped with a Cu $K_{\alpha 1,2}$ X-ray source. In the former case, each measurement was made within an angular range of 2θ = 8-80° or 8-120° and with a step of 0.0167°. In the latter case, the powder was packed in a 0.5 mm diameter capillary. The acquisition was performed in the 2θ range of 5° – 80° with a step size of 0.0167°. High angular resolution synchrotron X-ray powder diffraction (SXRPD) was performed at the MSPD beamline of ALBA synchrotron (Barcelona, Spain). The powders were packed in a 0.5 mm diameter capillary and mounted on the goniometer in Debye-Scherrer geometry. The data were recorded by using MYTHEN detector at a wavelength of 0.8251 Å, in the 2θ angular range of 0.34^o - 72^o with a 0.006^o step. The X-ray diffraction analysis was performed with FULLPROF suite for indexing the reflection lines and with JANA2006 for the refinements and calculations of Fourier difference maps. Note that in the following, when diffraction line widths are compared, it means that it is possible to do this comparison despite the use of different diffractometers. To keep a reasonable amount of parameters refined together during Rietveld refinements and avoid major correlations, the Fe, C and N sites were considered to be fully occupied and the B_{iso} parameters were fixed to reasonable values according to the covalency of the bonds in which these atoms are involved (B_{iso}-Fe = 0.5 $Å^2$, B_{iso}-C = B_{iso}-N = 0.7 $Å^2$ and B_{iso}-O = 1 $Å^2$.

Morphology characterization. Scanning electron microscopy (SEM) images were taken on the metallized samples (Pd-deposited) by a Hitachi Model S-4500 microscope.

Thermogravimetric analysis. Water content was determined using a TG/DTA SDT Q600 TA Instrument, the measurements were performed from room temperature to 600°C at 5°C/min in Ar atmosphere. TGA-MS analyses were performed on a SETARAM TAG 24 instrument, from room temperature until 450°C at 3°C/min in Ar atmosphere.

Mössbauer spectroscopy analyses. ^{57}Fe Mössbauer spectra were collected using a constant acceleration Halder-type spectrometer operating in transmission geometry with a room temperature ^{57}Co source (embedded in Rh matrix). The velocity scale was calibrated according to the ^{57}Fe Mössbauer spectrum of a pure α-Fe^0 foil recorded at room temperature. The refinement of Mössbauer hyperfine parameters (δ isomer shift, Δ quadrupole splitting, Γ signal line width and relative areas) was performed using both homemade programs and the WinNormos software (Wissenschaftliche Elektronik GmbH). In this study, when the signal was too broad (Γ > 0.40 mm/s) a distribution of the quadrupole splitting parameters (Δ) was used following the method proposed by Hesse and Rübartsch.[20]

Electrochemical characterization. Electrochemical performance of the materials was tested in CR2032-type coin cells. The positive electrode was prepared as a slurry containing 85 wt.% active material, 10 wt.% Ketjen black (KB), and 5 wt.% polyvinylidene fluoride (PVDF, Fluka, M 534.0) dispersed in N-methyl-2-pyrrolidone (NMP, Sigma-Aldrich; ≥ 99%) casted on an Al foil with the doctor blade technique. The films as obtained were then dried at 80°C overnight in an oven to evaporate NMP. The electrodes were then cut as 14 mm diameter discs, pressed under 5 T and finally dried at 80°C in vacuum, except for the dehydrated phase which were dehydrated at 220 °C for 2h as described in reference 18. The mass loading of the as-prepared electrode was around 2 to 3 mg.cm^{-2}. A homemade electrolyte which contained 1M solution of $NaPF_6$ (Strem Chemical; 99%) in propylene carbonate (PC) (Sigma-Aldrich; ≥ 99.7%) with 2 wt.% of fluoroethylene carbonate (FEC) (Sigma-Aldrich; ≥ 99%) was used for

all the electrochemical tests. The assembled cells were cycled in galvanostatic mode, at a C/20 (4.25mA/g) cycling rate between 2 and 4.25/4.3 V vs. Na^+/Na.

3. Results and discussions

Morphological study

Scanning electron microscopy (SEM) has been used to study the morphology of the as-prepared materials. The SEM images of all materials are shown in **Figure 2**. As observed in **Figure 2a**, the Na-FeHCF-Cop-60°C powder consists of ca. 50 nm grains aggregated into larger particles of ca. 10 μm. The material synthesized at the same temperature by the hydrothermal route (Na-FeHCF-hyd-60°C) is characterized by a very different particles' morphology with the formation of cubes with very sharp edges of ca. 1-3 μm (**Figure 2b**). The rapid precipitation and nucleation observed for the coprecipitation route yielded to the formation of irregular aggregates containing small size particles. Although ascorbic acid, which was added into the two solutions of precursors $FeCl_2$ and $Na_4Fe(CN)_6$ as an antioxidant, is also a chelating agent, its concentration was here not high enough to slow down nucleation versus growth.[19] On the contrary, for hydrothermal syntheses, $Na_4Fe(CN)_6$ is used as a single precursor in the presence of a large excess of ascorbic acid (4.5 equivalents) that acts here as antioxidant and chelating agent boosting the growth process towards the formation of micrometric well-shaped cubic particles.

The comparison of the materials synthesized by the hydrothermal route at different temperatures (Na-FeHCF-hyd-60°C, Na-FeHCF-hyd-107°C and Na-FeHCF-hyd-140°C) is given in **Figures 2b-d**. It appears that the temperature does not affect the shape and size of the

materials' particles, as in all cases the powder exhibits cubic-shaped particles with edges of ca. 1-3 μm.

The Na-FeHCF-reflux-107°C material was synthesized differently from those described before, despite similar precursors and concentrations to the hydrothermal synthesis. This synthesis took place in air, and the precursors, ($Na_4Fe(CN)_6$ and ascorbic acid, were mixed and then heated at 107°C under reflux. Ascorbic acid as chelating agent promoted growth versus nucleation, as shown by the even bigger cubic-shaped particles obtained (ca. 5 μm) (**Figure 2e**) (See **Figure S1** in the supporting information for a more general view of the powder). This result highlights that the difference in pressure between the reflux and hydrothermal conditions has a clear impact on the particles' size.

Figure 2f shows that the material obtained from dehydration of Na-FeHCF-reflux-107°C at 220°C in vacuum, is characterized by similar particles, in shape (cubic) and in size (ca. 5 μm) than its precursor (See **Figure S1** in the supporting information for a more general view of the powder), suggesting that the dehydration process do not have any impact on the morphology. However,

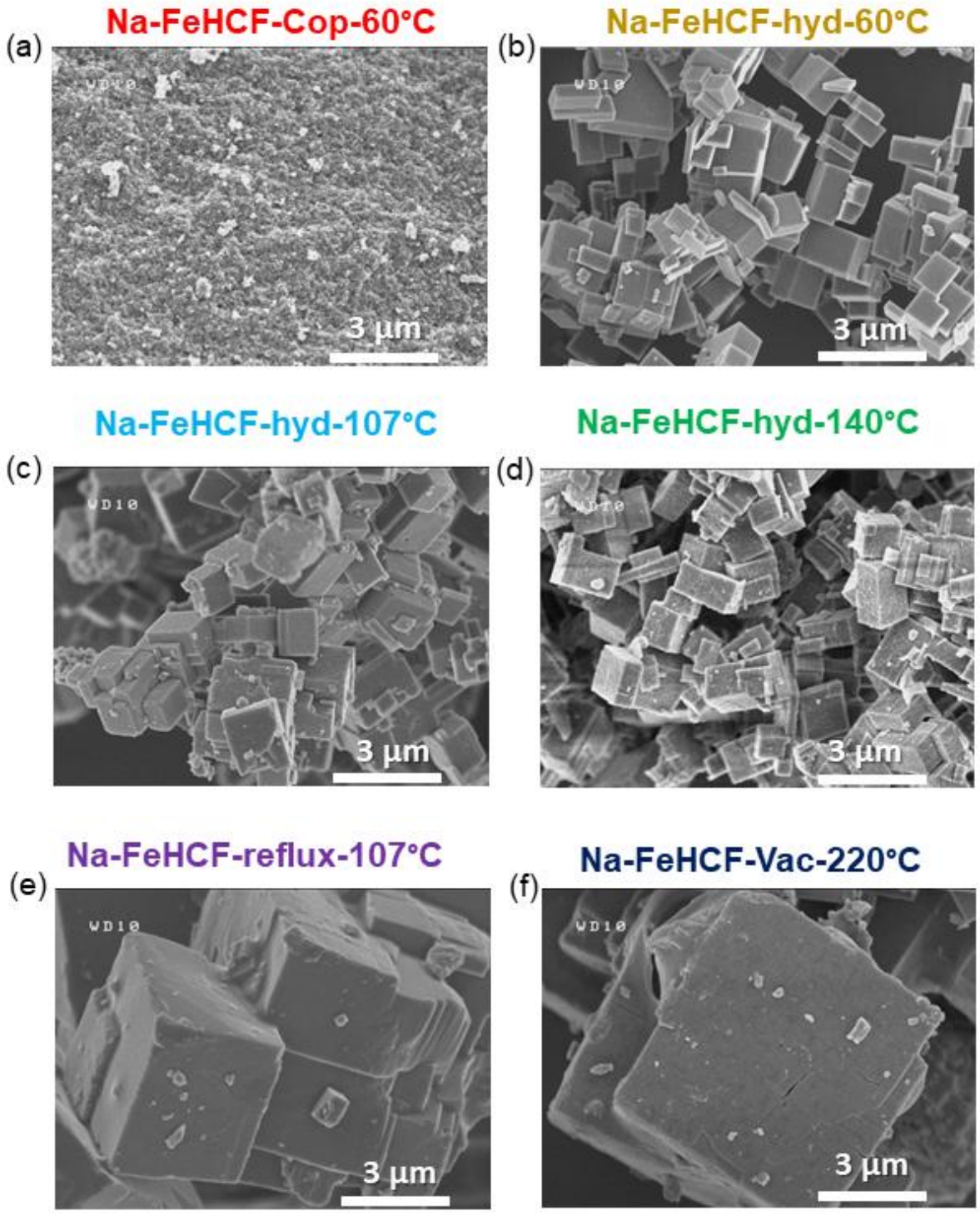

Figure 2: SEM images of the 6 different Na-FeHCF materials. Scale bar is 3 µm.

Thermogravimetric analyses

Thermogravimetric analyses coupled with mass spectrometry (TGA-MS) were performed for all materials in order to determine their content in water and their decomposition temperature. For all of them, the decomposition starts in the 200-250°C temperature range, as highlighted by the release of HCN and CO_2 (see **Figure S2** in supplementary information for more details).

TGA-MS of Na-FeHCF-Cop-60°C revealed no significant mass loss below 100°C, and about 10 wt.% at 200°C corresponding to 1.6 water molecules. However, for the material synthesized at the same temperature by the hydrothermal route (Na-FeHCF-hyd-60°C) a mass loss of only 8 wt.% is observed at 250°C, corresponding to 1.3 water molecules. This revealed changes in the water content for these two Na-FeHCF materials.

For the two other materials synthesized by the hydrothermal route at higher temperatures, the content in water varies from 3.4 to 4 wt.%, for Na-FeHCF-hyd-107°C and Na-FeHCF-hyd-140°C, respectively. It is thus worth highlighting that despite no modification of the shape and size of the particles the synthesis temperature has an effect on the water content in Na-FeHCF.

Again, despite similar synthesis temperatures for both materials, Na-FeHCF-reflux-107°C and Na-FeHCF-hyd-107°C, a mass loss of 10 wt.% was observed for the former whereas only 3.4 wt.% for the latter. This corresponds to two water molecules per formula unit for Na-FeHCF-reflux-107°C and to only 0.59 for Na-FeHCF-hyd-107°C. This highlights again the impact of synthesis routes and conditions not only on the morphology but also on the composition of the NaFeHCF materials.

As expected, Na-FeHCF-Vac-220°C obtained by dehydration of Na-FeHCF-reflux-107°C shows the smallest loss of water with only 1 wt.% at 250°C.

Structural description

The XRPD patterns of all materials are displayed in **Figure 3**. It can be observed that a pattern with less diffraction peaks, in good agreement with a higher symmetry of the structure, is observed for the materials synthesized at low temperatures, while for higher temperatures a deviation from a cubic-profile pattern occurs. This deviation from the cubic symmetry would be, as reported in literature [9], a confirmation of the higher amount of Na in the structure. Moreover, a difference in the line width can be observed depending on the synthesis route as discussed below.

The XRPD patterns of the two samples prepared at 60°C can be indexed in the cubic *Fm-3m* space group, but exhibit very different diffraction line width. Note that the Na-FeHCF-Cop-60°C phase also exhibits an extra peak at Q=2.25 $Å^{-1}$ attributed to an unknown impurity **(Figure 3a and Figure S3).** The full width at half maximum (FWHM) of the three first diffraction peaks corresponding to the (200), (220) and (400) reflection planes are 0.233, 0.295 and 0.297°(2θ) for Na-FeHCF-Cop-60°C and approximately 5 times narrower for Na-FeHCF-hyd-60°C (0.0418, 0.0627 and 0.0579°) (**Figure 3b**). This difference is mainly due to the very different crystallites' size of the two samples, as supported by the SEM analysis previously discussed. The refined cell parameter of the Na-FeHCF-Cop-60°C phase, a = 10.2585(4) Å, is different from the value a = 10.350(5) Å reported by Piernas-Munoz *et al.* [17], but we report better reliability factors here. The main diffraction peaks for the Na-FeHCF-hyd-60°C phase are located at lower angles compared to the ones of Na-FeHCF-Cop-60°C, in agreement with the refined slightly larger lattice parameter value, a=10.33939(7) Å. A high quality Rietveld refinement was performed for this sample thanks to its high crystallinity and the results are described in details in **Figure S4** and **Table S5**. The occupancy of the Na and O sites, the latter corresponding to the localization of the O atom of the water molecule H_2O,

was determined allowing then to propose the chemical formula **$Na_{1.36}Fe_2(CN)_6 \cdot 1.86H_2O$** (see **Table S6** in supplementary information).

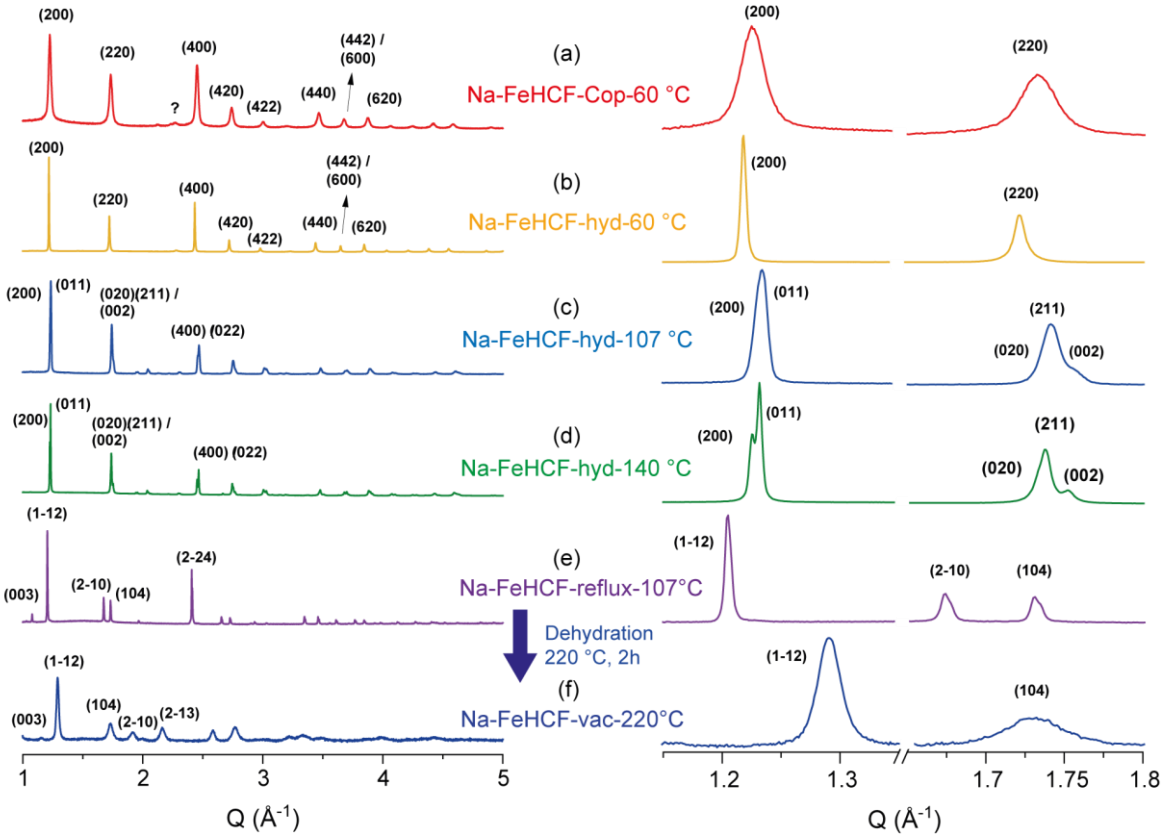

Figure 3: X-ray powder diffraction (XRPD) patterns for Na-FeHCF-Cop-60°C (red), Na-FeHCF-Vac-220°C (blue-dark), Na-FeHCF-hyd-107°C (blue-light), Na-FeHCF-reflux-107°C (purple) and SXRPD data recorded for Na-FeHCF-hyd-60°C (yellow), Na-FeHCF-hyd-140°C (green). Insets show enlargements of the (1.1-1.4) and (1.60-1.85) Q ranges ($Å^{-1}$). (Q space is used to account for the different wavelengths used, with $Q = 4\pi/\lambda * \sin\theta$).

Note that we did not refine all occupancies and thermal displacement factors (B_{iso}) in order to not overfit the experimental data. The Fe, C and N sites were considered to be fully occupied and the B_{iso} parameters were fixed to reasonable values according to the covalence of the bonds in which these atoms are involved (B_{iso}-Fe = 0.5 $Å^2$, B_{iso}-C = B_{iso}-N = 0.7 $Å^2$ and B_{iso}-O = 1 $Å^2$).

In order to understand the effect of the temperature using the hydrothermal route, the materials Na-FeHCF-hyd-107°C and Na-FeHCF-hyd-140°C were synthesized using same conditions as for Na-FeHCF-hyd-60°C but with different temperatures. The XRPD and the SXRPD patterns of Na-FeHCF-hyd-107°C and Na-FeHCF-hyd-140°C are shown in **Figures 3c and 3d**, respectively. In good agreement with the discussion on the particles size, they all exhibit sharp diffraction lines. The XRPD and SXRPD patterns of Na-FeHCF-hyd-107°C and Na-FeHCF-hyd-140°C exhibit a splitting of the main peaks in contrast to the material synthesized in the same conditions but at 60°C, suggesting an orthorhombic distortion of the unit cell. For instance, the first diffraction peak $(200)_{Fm\text{-}3m}$ is now shifted towards higher angles and split into two lines, corresponding to the crystallographic planes (200) and (011) in an orthorhombic unit cell, as clearly observed in the SXRPD pattern of Na-FeHCF-hyd-140°C. Similar observation is made for the second diffraction peak $(220)_{Fm\text{-}3m}$, also shifted towards higher angles and split into three lines, corresponding to the crystallographic planes (020), (211) and (002) in an orthorhombic unit cell. This orthorhombic distortion is observed in both patterns as shown in **Figure S7**.

The SXRPD pattern of Na-FeHCF-hyd-140°C was initially indexed in the $Pmn2_1$ orthorhombic space group to determine the unit cell parameters: a = 10.23550 (1) Å, b = 7.24140 (7) Å and c = 7.15920 (8) Å. Satisfactory reliability factors were obtained for this full pattern matching refinement (RBragg = 5.76, Rp = 1.76, Rwp = 3.35) (see **Figure 4**), but other orthorhombic space groups such as *Pmmm* gave similar results (as illustrated in **Figure S8**). Even though *Pmmm* is of higher symmetry, $Pmn2_1$ is probably more appropriate. Indeed, four distinct iron sites are needed to describe the PBA framework in the *Pmmm* space group whereas only two are needed in the $Pmn2_1$ space group. Provided that two Fe sites were identified by Mössbauer spectroscopy as discussed hereafter, we tried to solve the structure by

ab initio in the *Pmn2₁* space group. However, the structural description could not be achieved successfully as discussed in details in **Figure S9** in supplementary information. This orthorhombic phase is a new polymorph of $Na_2Fe_2(CN)_6$, isostructural to the potassium derivative $K_2Fe_2(CN)_6 \cdot 2H_2O$ described in the space group *Pmn2₁* with lattice parameters a = 10.06 Å, b = 7.27 Å and c = 7.12 Å.[21] Note that the structural description of this potassium polymorph is not available either. The two hydrothermal samples synthetized at 107°C and 140°C can be described with the same unit cells and the corresponding lattice parameters are given in **Table 1**.

Table 1 : Cell parameters of Na-FeHCFs materials obtained from refinement of the X-ray powder diffraction data.

Material	Lattice parameters	Space group	Crystal system
Na-FeHCF-Cop-60°C	a = b = c = 10.2585(4) Å	Fm-3m	Cubic
Na-FeHCF-hyd-60°C	a = b = c= 10.33939(7) Å	Fm-3m	Cubic
Na-FeHCF-hyd-107°C	a = 10.2361(2) Å b = 7.2465(3) Å c = 7.1664(2) Å	$Pmn2_1$ *	Orthorhombic
Na-FeHCF-hyd-140°C	a = 10.23550(1) Å b = 7.24140(7) Å c = 7.15920(8) Å	$Pmn2_1$ *	Orthorhombic
Na-FeHCF-reflux-107°C	a = b = 7.5111(2) Å c = 17.5086(6) Å	R-3	Rhombohedral
Na-FeHCF-Vac-220°C	a = b = 6.537(1) Å c = 18.888(3) Å	R-3	Rhombohedral

* Orthorhombic space group proposed based on the information obtained on the number of Fe environments by Mössbauer spectroscopy

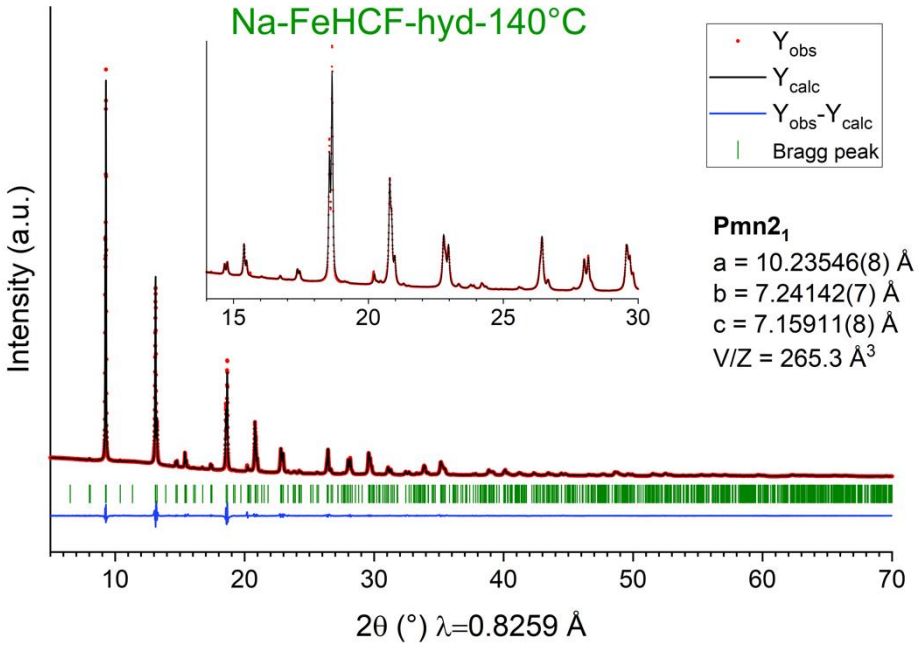

Figure 4: Full pattern matching refinement of the SXRPD data recorded for *Na-FeHCF-hyd-140°C*, performed in the ***Pmn2$_1$*** space group. Insets show the different peaks characterizing the orthorhombic distortion.

The XRPD pattern collected for Na-FeHCF-reflux-107°C appears also quite different from that of Na-FeHCF-hyd-107°C synthesized by the hydrothermal synthesis route at the same temperature. The pattern of Na-FeHCF-reflux-107°C is similar to the one described by some of us in reference 18 and was indexed at that time in the *P2$_1$/n* space group. However, it appears also fully indexed by the higher symmetry rhombohedral *R-3* space group, with the lattice parameters a = b = 7.5111(2) Å and c = 17.5086(6) Å. While the first diffraction peak that corresponds to the $(1\text{-}12)_{R\text{-}3}$ crystallographic plane shifted towards lower angles, two diffraction peaks instead of one are observed in the Q range (1.65-1.85) ($Å^{-1}$), corresponding to the $(2\text{-}10)_{R\text{-}3}$ and $(104)_{R\text{-}3}$ crystallographic planes as displayed in **Figure 3e**. The Rietveld refinement performed in the rhombohedral unit cell is described in **Figure 5** and **Table 2**. In this description, all the carbon or nitrogen sites are equivalent, hence all the Fe-C or Fe-N

bonds are identical and determined to be equal to 1.940(4) Å and 2.156(2) Å respectively. This result is in agreement with the Mössbauer spectroscopy analysis discussed later in this paper. The position of the water molecules was determined using Fourier difference maps (**Figure 6**) and associated with an occupancy of 0.64, corresponding to ~2 water molecules per formula unit. Two oxygen sites were identified at the center of the faces of the large pseudo cubic cages, associated to significantly different electronic densities as can be seen on the cross section of the electron density isosurfaces. This suggests a different occupancy for the two H_2O sites. However, we were not able to correctly refine the structure considering these two independent sites and their occupancy due to the limited amount of parameters that can be refined at once: only an average one could be considered to describe the two sites. Finally, the refinement of sodium site occupancy allowed to propose the chemical formula **$Na_{1.86}Fe_2(CN)_6 \cdot 1.92H_2O$** (see **Table S6** in supplementary information).

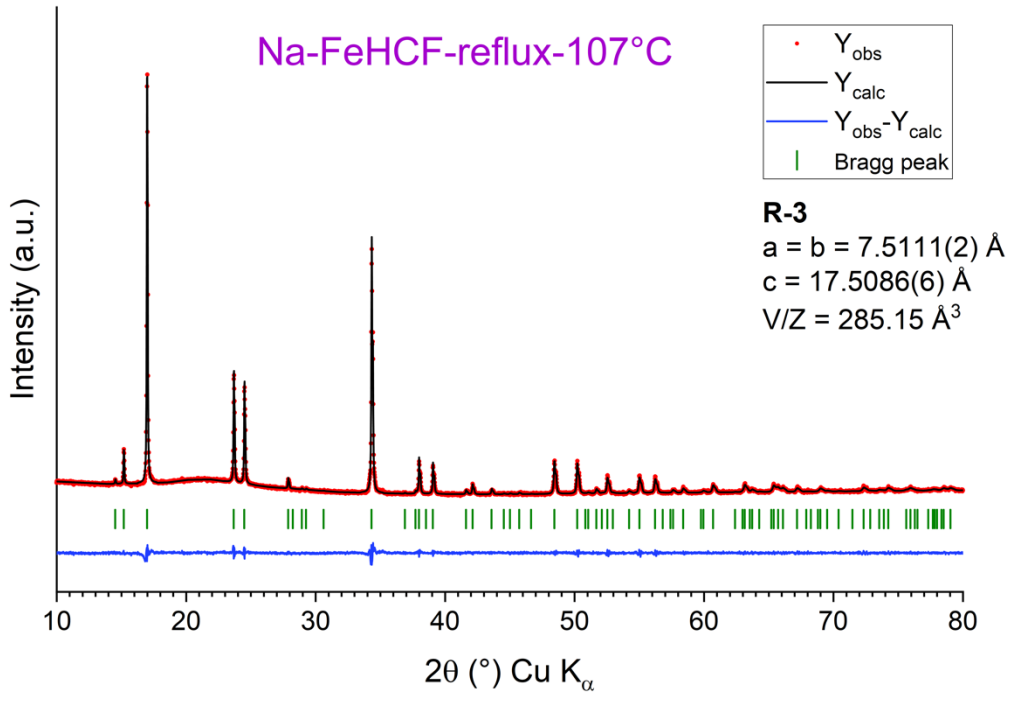

Figure 5: Result of the Rietveld refinement performed in the **R-3** space group of the X-ray powder diffraction data recorded for Na-FeHCF-reflux-107°C.

Table 2: Atomic coordinates and main interatomic distances determined from the Rietveld refinement performed in the **R-3** space group of the X-ray powder diffraction data recorded for Na-FeHCF-reflux-107°C.

$Na_{1.86}Fe_2(CN)_6 \cdot 1.92H_2O$						
S.G. **R-3** *Z* = 3		*a* = *b* = 7.511(2) Å c = 17.5086(6) Å *V/Z* = 285.15 Å^3				R_{Bragg} = 1.82 R_p = 0.61 R_{wp} = 0.90
Atoms	**Wyckoff positions**	***x/a***	***y/b***	***z/c***	**Occupancy**	**B_{iso}**
Fe (1)	3a	0	0	0	1	0.5
Fe (2)	3b	1/3	2/3	1/6	1	0.5
Na	6c	0	0	0.251(2)	0.93(3)	2.4(3)
C	18f	0.122(2)	0.868(2)	0.0582(4)	1	0.7
N	18f	0.219(1)	0.810(1)	0.0939(4)	1	0.7
O	9e	1/3	1/6	1/6	0.64(1)	1

Bond	**Distance (Å)**
Fe (1) - C	1.940(4)
Fe (2) - N	2.156(2)
C - N	1.152(6)
Na - O	2.604(7)

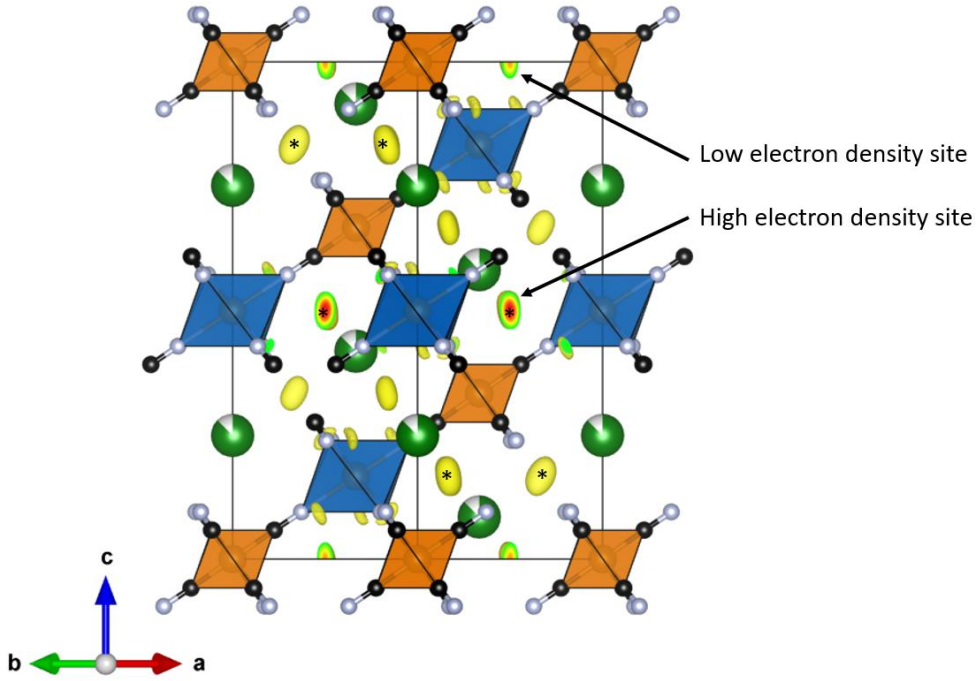

Figure 6: Result for Na-FeHCF-reflux-107°C of the Fourier difference map calculated after the Rietveld refinement of XRD data without considering the oxygen atoms of the interstitial H_2O. The two possible H_2O sites are displayed in yellow and red.

As described in reference 18, Na-FeHCF-reflux-107°C can be dehydrated thermally and under vacuum to obtain the rhombohedral phase described first by Wang *et al.*[16] In this work, the XRPD pattern of the corresponding material, Na-FeHCF-Vac-220°C, is displayed in **Figure 3f**. It can be unambiguously indexed in a rhombohedral symmetry as demonstrated in **Figures S10** and **S11**. All the observed diffraction peaks can be indexed in the *R-3* space group with lattice parameters (a = b = 6.5437(1) Å and c = 18.888(3) Å) very similar to those reported by Wang *et al.* (a = b = 6.548(1) Å and c = 18.931(3) Å). Furthermore, this XRD pattern exhibits very broad diffraction peaks, as for Na-FeHCF-Cop-60°C. For instance, the linewidths FWHM of the first three diffraction peaks of the XRPD pattern of Na-FeHCF-Vac-220°C (**Figure 3f**) are 0.326, 0.629 and 0.644°(2θ) corresponding to (1-12), (104) and (2-10) crystallographic planes respectively, while much sharper linewidths (0.066, 0.077 and

0.074°(2θ)) were observed for Na-FeHCF-reflux-107°C before dehydration (**Figure 3e)**. Here, the broad diffraction peaks observed in the XRPD pattern of Na-FeHCF-Vac-220°C cannot be attributed to the nanometer size of the particles as for Na-FeHCF-Cop-60°C, since they are micrometer sized. The broadening can be tentatively attributed to a disorder leading to a reduction of the coherent domains in the particles versus the pristine hydrated precursor Na-FeHCF-reflux-107°C. Indeed, according to the coherent length calculations using the Scherrer law, the average size of diffracting domains was shown to be reduced from ~3 µm to ~150 nm for Na-FeHCF-reflux-107°C and Na-FeHCF-Vac-220°C respectively.

Mössbauer spectroscopy analyses

Room temperature Mössbauer spectra of all materials are displayed in **Figure 7** and the corresponding refined hyperfine parameters of each component are reported in **Table 3**. They all exhibit a singlet at ~ δ = -0.12 mm/s corresponding to six-fold coordinated LS-Fe^{2+} [22] and representing between 40 and 50 % of the spectrum global area: ~40 % for Na-FeHCF samples synthesized at low temperature (60°C) and ~ 50 % for all the other materials. This apparent singlet may indeed be considered as a quadrupole doublet with a very low value of the quadrupole splitting parameter ($\Delta \leq 0.13$ mm/s) as it is expected for LS-Fe^{2+} Mössbauer signal. Note, that this splitting is slightly weaker ($\Delta \leq 0.05$ mm/s) for the NaFeHCF-hyd-107°C and NaFeHCF-hyd-140°C materials compared to others, reflecting slightly less local distortion on those phases.

All spectra, as shown in **Figure 7**, exhibit one or two additional components depending on the synthesis conditions used to prepare the Na-FeHCF materials. For Na-FeHCF-Cop-60°C, the Mössbauer spectrum can be described as the sum of an apparent singlet at δ = -0.13 mm/s, a broad and unresolved signal centered at $\delta \approx 0.38$ mm/s and a quadrupole doublet of very low

intensity with a high isomer shift value (δ = 1.11 mm/s) and a large quadrupole splitting (Δ = 1.17 mm/s), attributed to LS-Fe^{2+} (41 %), HS-Fe^{3+} (57 %) and HS-Fe^{2+} (2%), respectively. The detection of a trivalent iron signal implies that this Na-FeHCF material may be Na^+-deficient. It has been recently proposed by Ojwang *et al* in ref. 23 that it could be due to reactivity with moisture. However, in our case, Mössbauer data were promptly collected after the synthesis putting special care in avoiding possible moisture. Moreover, the corresponding Fe^{3+} sub-spectrum is characterized by a distribution of the quadrupole splitting hyperfine parameter (inset of **figure 7a**), suggesting a series of different local environments for HS-Fe^{3+} with different site distortions depending on the distribution on the adjacent cationic sites (Fe/vacancy and Na/vacancy) and/or structural water molecules.

The Na-FeHCF materials prepared by the hydrothermal route (Na-FeHCF-hyd-60°C, Na-FeHCF-hyd-107°C and Na-FeHCF-hyd-140°C) exhibit Mössbauer spectra that differ significantly depending on the synthesis temperature. For Na-FeHCF-hyd-60°C, in addition to the LS-Fe^{2+} sub-spectrum (38%), two quadrupole doublets assigned to HS-Fe^{2+} (35%) and HS-Fe^{3+} (27%) are observed at δ = 1.06 mm/s and δ = 0.37 mm/s, respectively. In contrast, the amount of HS-Fe^{3+} is reduced to 5 % for Na-FeHCF-hyd-107°C and 0% for Na-FeHCF-hyd-140°C, while the amount of HS-Fe^{2+} increases from 46 to 50 %, respectively. Therefore, as the temperature used during the synthesis increases, the amount of HS-Fe^{3+} decreases indicating larger content of Na^+ ions within the structure. Finally, the material synthesized at 140°C appears to be really stoichiometric with a composition in Na, Fe and CN such as **$Na_2Fe_2(CN)_6$**.

The Na-FeHCF-reflux-107°C material exhibits an additional doublet, observed at δ = 1.12 mm/s corresponding to HS-Fe^{2+} (50%), this signal is very similar to that observed in the Mössbauer spectrum of Na-FeHCF-hyd-140°C suggesting also that the synthesis of a perfectly stoichiometric material has been achieved. In contrast, for Na-FeHCF-Vac-220°C,

the HS-Fe^{2+} sub-spectrum (δ = 1.12 mm/s) is satisfactorily described by a bi-modal distribution of quadrupole doublets (inset of **figure 7f**) suggesting two different disordered environments for HS-Fe^{2+}. A similar and broader Δ distribution was also evidenced for high-spin divalent iron in the Na-FeHCF-hyd-60°C material that presents as its analogue Na-FeHCF-cop-60°C, the highest Na^+ deficiency (**figure 7b**). Thus, the Na-FeHCF compound prepared under vacuum at 220°C may also be slightly Na^+-deficient, what is consistent with the detection of a low-intensity (7% in relative area) quadrupole doublet (δ = 0.41 mm/s, Δ = 0.57 mm/s) associated with HS-Fe^{3+}.

In conclusion, the different synthesis methods do have a clear impact on the ratio LS-Fe^{2+} / HS-Fe^{2+}, presence of HS-Fe^{3+} (due to Na deficiency) and local disorder around Fe species Fe^{2+} / Fe^{3+}. Overall, only the Na-FeHCF-hyd-140°C material appears to present the ideal LS-Fe^{2+} / HS-Fe^{2+} ratio (50/50) with the weakest disorder of the Fe environments.

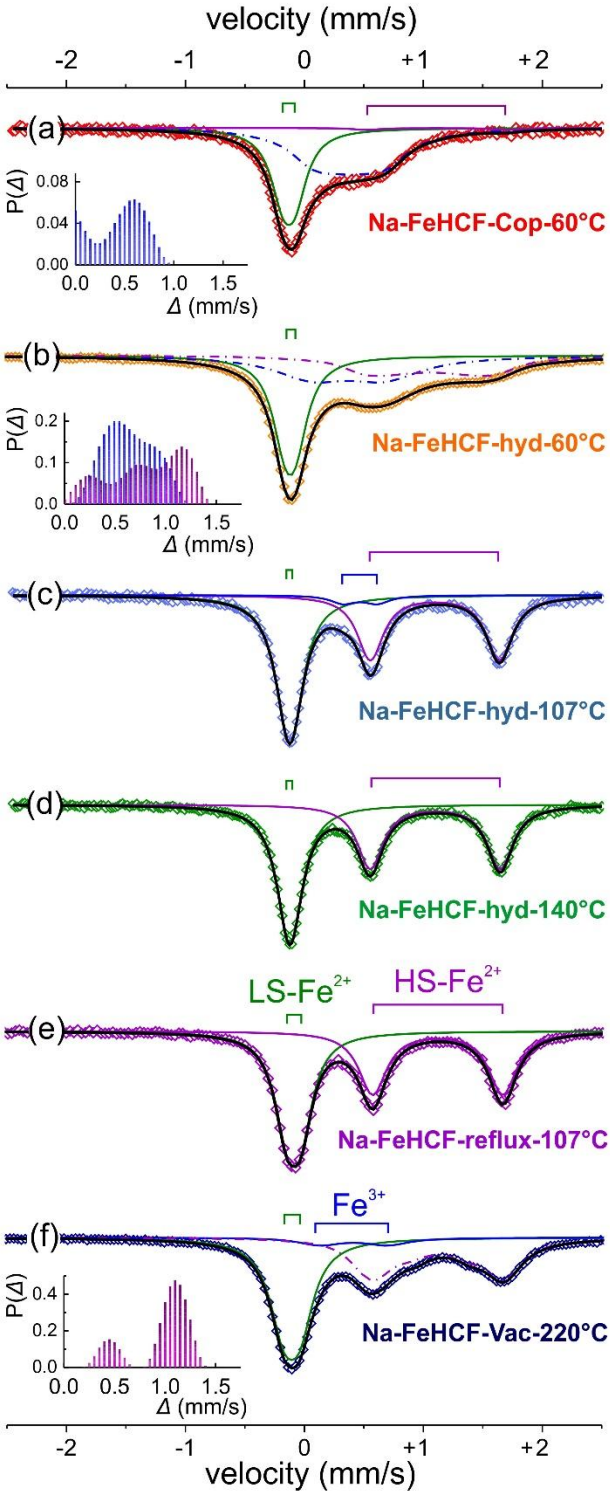

Figure 7*:* Room temperature ^{57}Fe Mössbauer spectra of Na-FeHCF samples. Sub-spectra with dashed lines were calculated using a distribution of the quadrupole splitting (Δ) hyperfine parameter (given in insets).

Table 3: Refined room temperature ^{57}Fe Mössbauer hyperfine parameters for Na-FeHCF samples (δ isomer shift in respect to α-Fe, Δ quadrupole splitting, Γ Lorentzian line width and A relative area). (*) mean value of the Δ distribution.

	δ (mm/s)	Δ (mm/s)	Γ (mm/s)	area (%)	assignement
(a) Na-FeHCF-Cop-60°C					
Site (1)	-0.13(1)	0.10(2)	0.25(3)	41(3)	LS-Fe^{2+}
Site (2)	1.11(8)	1.17(9)	0.30(4)	2(2)	HS-Fe^{2+}
Dist. (3)	0.38(6)	0.50*	0.30(-)	57(3)	HS-Fe^{3+}
(b) NaFeHCF-hyd-60°C					
Site (1)	-0.12(1)	0.09(1)	0.25(1)	38(2)	LS-Fe^{2+}
Dist. (2)	1.06(2)	0.88*	0.30(-)	35(3)	HS-Fe^{2+}
Dist. (3)	0.37(5)	0.61*	0.30(-)	27(3)	HS-Fe^{3+}
(c) NaFeHCF-hyd-107°C					
Site (1)	-0.12(1)	0.05(3)	0.25(1)	49(2)	LS-Fe^{2+}
Site (2)	1.10(1)	1.09(1)	0.27(1)	46(2)	HS-Fe^{2+}
Dist. (3)	0.47(2)	0.29(6)	0.26(4)	5(2)	HS-Fe^{3+}
(d) NaFeHCF-hyd-140°C					
Site (1)	-0.12(1)	0.03(3)	0.25(1)	50(2)	LS-Fe^{2+}
Site (2)	1.10(1)	1.09(2)	0.26(1)	50(2)	HS-Fe^{2+}
(e) NaFeHCF-reflux-107°C					
Site (1)	-0.09(1)	0.12(1)	0.24(1)	50(2)	LS-Fe^{2+}
Site (2)	1.12(2)	1.09(1)	0.28(1)	50(2)	HS-Fe^{2+}
(f) NaFeHCF-Vac-220°C					
Site (1)	-0.11(1)	0.13(2)	0.28(1)	49(2)	LS-Fe^{2+}
Dist. (2)	1.12(2)	0.98*	0.30(-)	44(2)	HS-Fe^{2+}
Site (3)	0.41(3)	0.57(7)	0.43(5)	7(2)	HS-Fe^{3+}

Electrochemical properties

The electrochemical performance of Na-FeHCFs materials were characterized in half cells in the 2.0 to 4.3 V *vs* Na^+/Na potential window. The electrochemical profiles obtained during the 1st and 2nd cycles and the corresponding derivatives of the 2nd cycles are displayed in **Figure 8**. Note that the Na-FeHCF-hyd-107°C was not studied due to its strong similarity with Na-FeHCF-hyd-140°C.

The two materials synthesized at 60°C, namely Na-FeHCF-Cop-60°C and Na-FeHCF-hyd-60°C, were shown to be non-stoichiometric samples combining XRPD and Mössbauer spectroscopy. This non-stoichiometry was supported (i) by the first electrochemical charge with the limited extraction of ~ 1.6 Na^+ ions and (ii) by the extra capacity observed during the next discharge and the subsequent charge during which ~ 2 Na^+ ions were intercalated first and then reversibly de-intercalated. The Na^+ deficiency in Na-FeHCF-Cop-60°C and Na-FeHCF-hyd-60°C was further supported by the insertion of 0.6 Na^+ into the structure when the Na cell is discharged first rather than being charged, as shown in **Figure S12** in the supporting information. Combining the information got from all the characterizations performed, the compositions $\mathbf{Na_{1.4}Fe_2(CN)_6 \cdot 1.6H_2O}$ and $\mathbf{Na_{1.4}Fe_2(CN)_6 \cdot 1.36H_2O}$ can be proposed for Na-FeHCF-Cop-60°C and Na-FeHCF-hyd-60°C respectively. This last composition is in agreement with the composition predicted by Rietveld refinement as shown in previous sections (as illustrated in **Table S6** in supplementary information). However, a small discrepancy in the amount of water can be shown between PXRD and TGA-MS analysis from 1.86 to 1.3 H_2O respectively. We believe that the right amount should be the one taken from the PXRD that allows better quantification of the oxygen associated with water molecules.

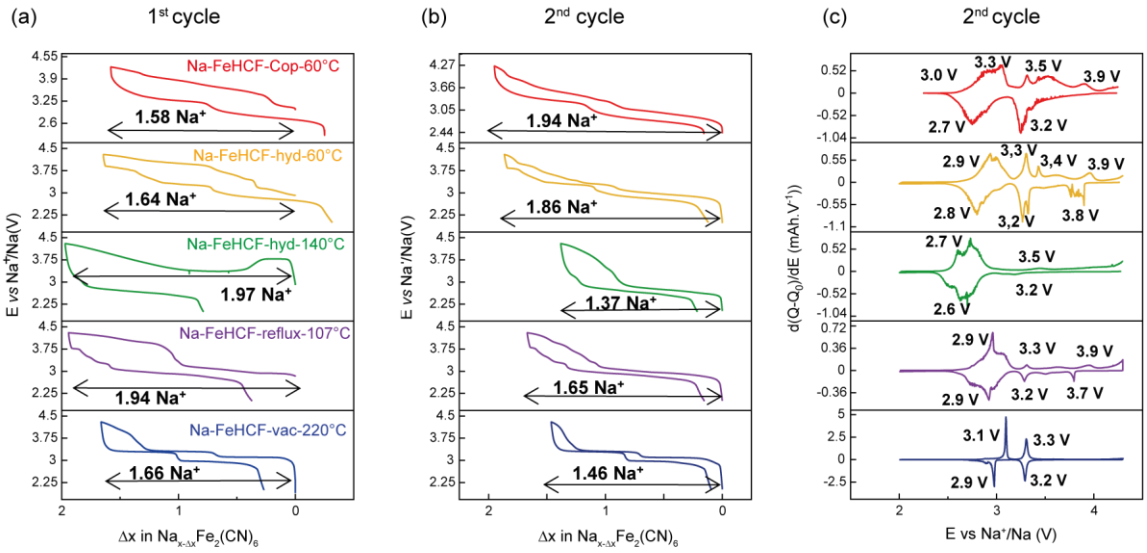

Figure 8: The electrochemical (*a*) 1st and (b) 2nd charge/discharge cycles of Na-FeHCF vs. Na metal, at the cycling rate of *C*/20 per Na^+, with the cut-off voltage of 4.3 V vs. Na^+/Na. (c) The second derivative charge/discharge curve as a function of the operational voltage. Δx correspond to the n° of Na exchange.

The main difference between Na-FeHCF-Cop-60°C and Na-FeHCF-hyd-60°C is the difference in the amount of water, and most probably the presence of $Fe(CN)_6$ vacancies in Na-FeHCF-Cop-60°C that could explain the large amount of Fe^{3+} (57%) detected by Mössbauer spectroscopy. It is worth noticing that the polarization observed during the first cycle of Na half cells with both materials Na-FeHCF-Cop-60°C and Na-FeHCF-hyd-60°C at the positive electrode is reduced during the second cycles. In both cases, the electrochemical curve became slopping suggesting that no formation of intermediate phases was observed during charge/ discharge. Despite very different particles' sizes, similar electrochemical behaviour is observed for the two compounds, suggesting no major influence of the particles' size onto the electrochemical performance in the conditions studied in this work. This is in contrast with observations made for potassium derivatives.[24]

In contrast, for the stoichiometric samples Na-FeHCF-hyd-140°C and Na-FeHCF-reflux-107°C, almost two Na^+ ions were extracted during the first charge confirming thus the rich Na content. A large polarization is observed during the first cycle of the battery, that is then reduced in subsequent cycles. Moreover, no extra capacity is observed in subsequent cycles and actually less Na^+ ions (1.37 and 1.65 Na^+ respectively) were re-intercalated within the structure after the first cycle. Finally, the sodium rich stoichiometry of these pristine materials is further evidenced by starting the Na half cells in discharge rather than in charge, resulting in a very limited intercalation of less to 0.2 Na^+ into the structure, as shown in **Figure S12**. Based on all the complementary information gathered, the compositions $\mathbf{Na_{1.8}Fe_2(CN)_6 \cdot 0.7H_2O}$ and $\mathbf{Na_{1.9}Fe_2(CN)_6 \cdot 2H_2O}$ could be proposed for Na-FeHCF-hyd-140°C and Na-FeHCF-reflux-107°C, respectively. This last composition is also in agreement with the composition estimated by Rietveld refinement (as illustrated in **Table S6** in supplementary information). The electrochemical curve observed for Na-FeHCF-hyd-140°C during the first charge of the Na cell exhibits a strange evolution in potential as function of the composition in Na. It results in a large irreversible capacity at the end of the first cycle. Despite unexpected, this electrochemical signature was shown to be reproducible as shown in **Figures 8** and **S12**. This feature is not understood yet and, although further experiments will be necessary to understand this behavior, it is interesting to point out that similar behavior was observed for iron hexacyanocobaltate materials as reported by Mullaliu *et al.* [25] A possible explanation could be the instability of the solid electrolyte interphase formed for Na rich or close to the stoichiometry phases with low content of water, as it has been proposed recently by Fu *et al.*[26] However, in our case, Na-FeHCF-Vac-220°C was shown to be the material with the smaller amount of water, and despite of that it does not show this strange electrochemical behavior during the first charge. This behavior remains thus to be fully understood.

Na-FeHCF-reflux-107°C has already been tested in different conditions: at different cycling rates, with different electrolytes as well as different binders etc.[18] Similar electrochemical performance were obtained with reversible capacities of 171 $mAh.g^{-1}$ and 148 $mAh.g^{-1}$ during the first charge in reference 12 and in this work, respectively.

The material Na-FeHCF-Vac-220°C is also stoichiometric as it has been shown by Mössbauer spectroscopy, with the detection of only 7% of HS-Fe^{3+}. When the Na half-cell is discharged first, rather than being charged, as expected only a very limited amount of Na^+ ions (0.04) was incorporated into the structure. Capacities of 142 $mAh.g^{-1}$ and 164 $mAh.g^{-1}$ are obtained when starting the Na cells in charge and in discharge, respectively. However, in any case, similar mechanisms are observed with two plateaus observed in the overall voltage range and with capacities similar to those already reported.[16, 18]

The derivative curves of the charge and discharge cycles calculated for all compounds are compared in **Figure 8c**. Several successive oxidation and reduction processes are observed for all Na-FeHCF materials, except for Na-FeHCF-hyd-140°C and Na-FeHCF-Vac-220°C which are characterized by only two processes. Sharp derivative peaks are observed only for Na-FeHCF-Vac-220°C, at 3.1 and 3.3 V in charge and at 2.9 and 3.2 V in discharge, in good agreement with references 10 and 12, suggesting the formation of an intermediate phase such as $Na_1Fe^{II}_{HS}Fe_{LS}^{III}(CN)_6$ before the full de-intercalation and the formation of $Fe_{HS}^{III}Fe_{LS}^{III}(CN)_6$.

The evolution of the discharge capacity over the first 5 cycles is compared in **Figure S13** for all Na-FeHCF materials. It can be observed that those containing less Na in their pristine state show higher reversible capacities versus those richer in Na. Nevertheless, only the latter can be used as positive electrode materials in Na-ion batteries, as the former require to be associated with a Na-containing negative electrode or Na metal.

4. Conclusion

The effect of the different synthesis conditions such as synthesis routes (coprecipitation, hydrothermal, under reflux and after a dehydration), temperatures, pressure and precursors was investigated in this work. It was determined that the higher the synthesis temperature the higher is the Na content and the smaller is the amount of water in the structure, with no changes in the morphology for the hydrothermal synthesis. Furthermore, slowing down the reaction using an excess of ascorbic acid favors the formation of Na-rich phases with cubic shape morphologies. Clearly, synthesis conditions have to be carefully chosen to obtain specific compositions and morphologies. Each synthesis method presented its pros and cons: even if the coprecipitation method seems really very easy to implement since no specific equipment is required, it requires a precise control of the concentrations and feeding rates under an inert atmosphere, in order to control the particle's composition and size, as two solutions of reactants are needed. In contrast, the reflux and hydrothermal synthesis routes can be easier to implement as a single solution of precursor is used, but these synthesis routes might be less scalable for industrial production. In the latter case, the excess (4.5 equivalent) of ascorbic acid acts as antioxidant and chelating agent reducing the nucleation rate and allowing a better control of the composition and particle' size.

A variety of Na-FeHCF compounds were prepared showing different structures described in three different unit cells of cubic, orthorhombic or rhombohedral symmetry, variable compositions in sodium, water and cationic vacancies, and a variety of morphologies. Some of these Na-FeHCF were already reported in the literature, nevertheless it is worth mentioning that one polymorph is reported for the first time, an orthorhombic phase with composition $Na_{\sim 1.8}Fe_2(CN)_6.0.7H_2O$ synthesized by an hydrothermal route at 140°C; while the structure of

another is also better described, the monoclinic phase obtained under reflux at 107°C, already reported by some of us [12], appears finally better described in a rhombohedral symmetry. When this material, revealed to be $Na_{1.86}Fe_2(CN)_6 \cdot 2H_2O$, was dehydrated, the same symmetry is maintained despite significant change in the cell parameters due to the release of water molecules. Mössbauer spectroscopy appears as crucial to characterize these Na-FeHCF materials, as allowing to get information, on the material's composition, but also on the Fe oxidation state and on the disorder around it.

All these materials Na-FeHCF were compared in Na half-cells in similar conditions (electrolyte, electrode formulation, potential window, cycling rate, etc.), starting in charge and in discharge, in order to get complementary information on the effect of the stoichiometry on the electrochemical properties of these PBAs.

This work participates to the better understanding of the impact of the synthesis conditions on Na-FeHCF in the frame of optimizing alternative low cost and sustainable electrode materials for future battery generation.

Author information:

Corresponding Authors:

*E-mail: Dany.Carlier@icmcb.cnrs.fr

*E-mail: Laurence.Croguennec@icmcb.cnrs.fr

Notes

The authors declare no competing financial interest.

Supporting Information

Supporting Information gives additional results on characterizations performed by scanning electron microscopy, thermogravimetric analysis coupled to mass spectrometry, X-ray diffraction, and electrochemical tests in half-cells versus Na metal.

Acknowledgements

The authors thank the RS2E Network for the funding of PSC's postdoctoral fellowship, as well as the financial support of CNRS (PEPS2017-Cellule Energie), Région Nouvelle Aquitaine, the French National Research Agency (STORE-EX Labex Project ANR-10-LABX-76-01) and the H2020 European Program (Project NAIADES). The authors also thank Eric LEBRAUD and Stan PECHEV, Philippe DAGAULT, Dominique DENUX and Catherine DENAGE (ICMCB-CNRS) for their help with XRD, TGA, TGA-MS and SEM analyses, respectively.

References

1. Dunn, B.; Kamath H.; Tarascon, J. M. Electrical Energy Storage for the Grid: A Battery of Choices. *Science* **2011**, 334, 928-935.

2. Palomares, V.; Serras, P.; Villaluenga, I.; Hueso, K. B.; Gonzalez, J. C.; Rojo, T. Na-ion batteries, recent advances and present challenges to become low cost energy storage systems. *Energy Environ. Sci*. **2012**, 5, 5884-5901.

3. Kundu, D.; Talaie, E.; Duffort, V.; Nazar, L. F. The emerging chemistry of sodium ion batteries for electrochemical energy storage. *Angew. Chem. Int. Ed*. **2015**, 54, 3431-3448.

4. Wang, R. Y.; Wessells, C. D.; Huggins, R. A.; Cui, Y. Highly Reversible Open Framework Nanoscale Electrodes for Divalent Ion Batteries. *Nano Lett*. **2013**, 13, 5748-5752.

5. Lipson, A. L.; Pan, B.; Lapidus, S. H.; Liao, C.; Vaughey, J. T.; Ingram, B. J. Rechargeable Ca-Ion Batteries: A New Energy Storage System. *Chem. Mater*. **2015**, 27, 8442-8447.

6. Mizuno, Y.; Okubo, M.; Hosono, E.; Kudo, T.; Oh-ishi, K.; Okazawa, A.; Kojima, N.; Kurono, R.; Nishimura, S.; Yamada, A. Electrochemical Mg^{2+} intercalation into a bimetallic CuFe Prussian blue analog in aqueous electrolytes. *J. Mater. Chem. A* **2013**, 1, 13055-13059.

7. Qian, J.; Wu, C.; Cao, Y.; Ma, Z.; Ma, Z.; Huang, Y.; Ai, X.; Yang, H. Prussian Blue Cathode Materials for Sodium-Ion Batteries and Other Ion Batteries. *Adv. Energy Mater*. **2018**, 1-24.

8. Lee, H.-W.; Wang, R. Y.; Pasta, M.; Lee, S. W.; Liu, N.; Cui, Y. Manganese hexacyanomanganate open framework as a high-capacity positive electrode material for sodium-ion batteries. *Nat. Commun*. **2014**, 5, 1-6.

9. Zhou, A.; Cheng, W.; Wang, W.; Zhao, Q.; Xie, J.; Zhang, W.; Gao, H.; Xue, L.; Li, J. Hexacyanoferrate-Type Prussian Blue Analogs: Principles and Advances Toward High-Performance Sodium and Potasium Ion Batteries. *Adv. Energy Mater*. **2021**, 11, 1-35.

10. Firouzi, A.; Qiao, R.; Motallebi, S.; Valencia, C. W. ; Israel, H. S.; Fujimoto, M.; Wray, L. A.; Chuang, Y.-D.; Yang, W.; Wessells, C. D. Monovalent manganese based anodes and co-solvent electrolyte for stable low-cost high-rate sodium-ion batteries. *Nat. Comm*. **2018**, 9, 1-10.

11. Song, J.; Wang, L.; Lu, Y.; Liu, J.; Guo, B.; Xiao, P.; Lee, J.-J.; Yang, X.-Q.; Henkelman, G.; Goodenough, J. B. Removal of Interstitial H_2O in Hexacyanometallates for a Superior Cathode of a Sodium-Ion Battery. *J. Am. Chem. Soc*. **2015**, 137, 2658-2664.

12. Wang, L.; Lu, Y.; Liu, J.; Xu, M.; Cheng, J.; Zhang, D.; Goodenough, J. B. A Superior Low-Cost Cathode for a Na-Ion Battery. *Angew. Chem. Int. Ed*. **2013**, 52, 1964-1967.

13. You, Y.; Yu, X.; Yin, Y.; Nam, K.; Guo, Y. Sodium iron hexacyanoferrate with high Na content as a Na-rich cathode material for Na-ion batteries. *Nano Res*. **2015**, 8, 117-128.

14. Li, W.-J; Chou, S.-L; Wang, J.-Z; Kang, Y.-M; Wang, J.-L; Liu, Y.; Gu, Q.-F; Liu, H.-K; Dou, S.-X. Facile Method To Synthesize Na-Enriched $Na_{1+x}FeFe(CN)_6$ Frameworks as Cathode with Superior Electrochemical Performance for Sodium-Ion Batteries. *Chem. Mater*. **2015**, 27, 1997-2003.

15. Wang, B.; Han, Y.; Wang, X.; Bahlawane, N.; Pan, H.; Yan, M.; Jiang, Y. Prussian Blue Analogs for Rechargeable Batteries. *iScience* **2018**, 3, 110-133.

16. Wang, L.; Song, J.; Qiao, R.; Wray, L. A.; Hossain, M. A.; Chuang, Y.-D.; Yang, W.; Lu, Y.; Evans, D.; Lee, J.-J.; Vail, S.; Zhao, X.; Nishijima, M.; Kakimoto, S.; Goodenough, J. B.

Rhombohedral Prussian White as cathode for Rechargeable Sodium-Ion Batteries. *J. Am. Chem. Soc*. **2015**, 137, 2548-2554.

17. Piernas-Munoz, M. J.; Castillo-Martinez, E.; Bondarchuk, O.; Armand, M.; Rojo, T.; Higher voltage plateau cubic Prussian White for Na-ion batteries. *J. Power Sources* **2016**, 324, 766-773.

18. Rudola, A.; Du, K.; Balaya, P. Monoclinic Sodium Iron Hexacyanoferrate Cathode and Non-Flammable Glyme-Based Electrolyte for Inexpensive Sodium-Ion Batteries. *J. Electrochem. Soc*. **2017**, 164, A1098-A1109.

19. Wang, W.; Gang, Y.; Hu, Z.; Yan, Z.; Li, W.; Li, Y.; Gu, Q.-F.; Wang, Z.; Chou, S.-L.; Liu, H.-K.; Dou, S.-X. Reversible structural evolution of sodium-rich rhombohedral Prussian blue for sodium-ion batteries. *Nat. Comm*. **2020**, 11, 1-9.

20. Hesse, J.; Rübartsch, A. Model independent evaluation of overlapped Mössbauer spectra. *J. Phys. E: Sci. Instrum.* **1974**, 7, 526-532.

21. Su, D.; McDonagh, A.; Qiao, S.-Z; Wang, G. High-Capacity Aqueous Potassium-Ion Batteries for Large-Scale Energy Storage. *Adv. Mater*. **2017**, 29, 3-8.

22. Samain, L.; Grandjean, F.; Long, G. J.; Martinetto, P.; Bordet, P.; Strivay, D. Relationship between the Synthesis of Prussian Blue Pigments, Their Color, Physical Properties, and Their Behavior in Paint Layers. *J. Phys. Chem. C* **2013**, 117, 9693-9712.

23. Ojwang, D. O.; Svensson, M.; Njel, C.; Mogensen, R.; Menon, A. S.; Ericsson, T.; Häggström, L.; Maibach, J.; Brant, W. R. Moisture-Driven Degradation Pathways in Prussian White Cathode Material for Sodium-Ion Batteries. *Appl. Mater. Interfaces* **2021**, 13, 10054-10063.

24. He, G.; Nazar, L. F. Crystallite Size Control of Prussian White Analogues for nonaqueous Potassium-Ion Batteries. *ACS Energy Lett*. **2017**, 2, 1122-1127.

25. Mullaliu, A.; Conti, P.; Aquilanti, G.; Plaisier, J. R.; Stievano, L.; Giorgetti, M. Operando XAFS and XRD Study of a Prussian Blue Analogue Cathode Material: Iron Hexacyanocobaltate. *Condens. Matter* **2018**, 3, 1-13.

26. Fu, H.; Xia, M.; Qi, R.; Liang, X.; Zhao, M.; Zhang, Z.; Lu, X.; Cao, G. Improved rate performance of Prussian blue cathode materials for sodium ion batteries induced by ion-conductive solid-electrolyte interphase layer. *J. Power Sources* **2018**, 399, 42-48.

Table Of Contents (TOC) graphic